Journal of Materials Chemistry A

Accepted Manuscript

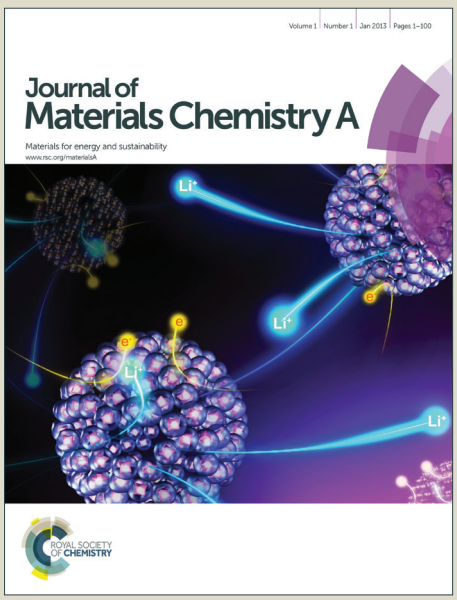

ROYAL SOCIETY OF CHEMISTRY

www.rsc.org/materialsA

Journal Name

RSCPublishing

COMMUNICATION

MoP is a Novel, Noble-Metal-Free Cocatalyst for Enhanced Photocatalytic Hydrogen Production in Water under Visible Light

Cite this: DOI: 10.1039/xoxxoooooox

Received ooth January 2012,
Accepted ooth January 2012

DOI: 10.1039/xoxxoooooox

www.rsc.org/

Qiudi Yue,[a] Yangyang Wan,[b] Zijun Sun,[a] Xiaojun Wu,*[b,c] Yupeng Yuan,[d] Pingwu Du*[a]

The generation of hydrogen (H_2) through photocatalytic water splitting with the employment of various cocatalysts has attracted much attention. Herein we report for the first time that metallic molybdenum phosphide (MoP), as a highly active cocatalyst, can significantly enhance photocatalytic H_2 production in water. A series of MoP/CdS nanorods (NRs) hybrids were facilely prepared. The optimal amount of MoP led to a maximal rate for H_2 evolution of 163.2 $\mu mol \cdot h^{-1} \cdot mg^{-1}$ under visible light illumination ($\lambda > 420$ nm), which is more than 20 times higher than that of freshly-prepared CdS NRs. This work demonstrated that the suitable Fermi level alignment of MoP and CdS is responsible for the high photocatalytic activity of H_2 production under visible light in the present system, as evidenced by both experimental and theoretical results.

The worldwide concerns of increasing energy demand and environmental issues due to the combustion of fossil fuels have highlighted the need for environmentally friendly and renewable energy carriers for our future energy supplies. H_2 production via water splitting is believed to be an ideal strategy to store solar energy and electricity.[1-5] Platinum[6, 7] and palladium[8, 9] are usually used as the cocatalysts for photocatalytic water splitting because of their excellent activities, but the high cost of these noble metals probably prohibits scaling up such systems for practical application.[10] Recently, noble-metal-free materials as the hydrogen evolution reaction (HER) cocatalysts have been widely studied for photocatalytic H_2 production in water, including $Ni(OH)_2$,[11] NiS,[12] MoS_2,[13] CoO_x[14], etc. According to Sabatier's principle,[15] the strong metal-hydrogen bonds on the surface of transition metals inhibit the hydrogen release from the active sites.[16] Interestingly, metal phosphides, due to the introduction of phosphorus (P), exhibit a weak "ligand effect" of metal-P bonds and a decreasing number of active metal sites because of the "ensemble effect" in the presence of P.[17-20] The structural alignment in metal phosphides can facilitate hydrogen release from the active sites. Recently, metal phosphides (e.g., Ni_2P,[21-23] $Ni_{12}P_5$,[24] Co_2P,[25] CoP,[26-29] FeP[30,31]) have been reported to show high activities and stabilities for HER. In our previous study, we also reported the use of Cu_3P as a p-type semiconductor to construct a novel p-n junction for photocatalytic H_2 production in water.[32] MoP was previously used as an active catalyst for hydrodesulfurization (HDS) and hydrodenitrogenation (HDN) reactions.[33-35] Due to the similarity of reversible binding of the catalyst and hydrogen atoms on the surface with respect to HDS and HER, MoP was also applied as electrocatalyst for HER, resulting in low onset overpotentials and small Tafel slopes.[36-40] Xiao *et al*. reported that MoP is a good "H delivery" system which can potentially modify the properties of the metal molybdenum, supporting the result with a combination of experimental results and theoretical calculations.[39] However, the introduction of MoP for photocatalytic H_2 production has not received prior investigation.

Inspired by above studies, herein we report for the first time noble-metal-free MoP as a highly active cocatalyst for photocatalytic H_2 production under visible light. MoP was synthesized from the molybdenum-based precursor by temperature programmed reduction (TPR) with linear temperature ramps in flowing reduction hydrogen. MoP displays a metallic character shown by a combination of both experimental data and density functional theory (DFT) analyses. In a hybrid MoP/CdS NRs metal-semiconductor system, the photocatalytic H_2 production activity under visible light was significantly enhanced. In addition, the results indicate that the suitable Fermi level alignment at the interface of MoP and CdS is responsible for efficient separation of photogenerated carriers in the present photocatalytic system.

MoP and CdS NRs were synthesized using a modified method of previous reports.[32, 38, 41] From the SEM image (Figure S1), we see that the morphology of MoP includes the presence of small nanoparticles of size 15-50 nm and some nanoparticles which are agglomerated. The commixture process was conducted by ultrasonicating CdS NRs with a certain amount of MoP in ethanol at room temperature for 60 minutes, followed by drying at 80 °C under N_2. Then the obtained solid samples were ground in an agate mortar

for 30 minutes, then were calcined at 200 °C under argon for 5 hours. The details can be found in the experimental section. As shown in Figures 1a, the SEM image of the hybrid MoP/CdS NRs sample reveals that the MoP nanoparticles are successfully attached onto the surface of the CdS NRs. CdS NRs show a length of 0.3-1.5 μm and a diameter at 40-90 nm. The MoP/CdS NRs morphology is also confirmed by transmission electron microscope (TEM) (Figure 1b and Figure S2), demonstrating similar shapes and sizes as that observed in SEM. The freshly-prepared CdS NRs and the CdS NRs after grinding and calcining show no significant morphological difference except that shorter and more disordered nanorods are present due to the grinding and sintering processes (Figure S3).

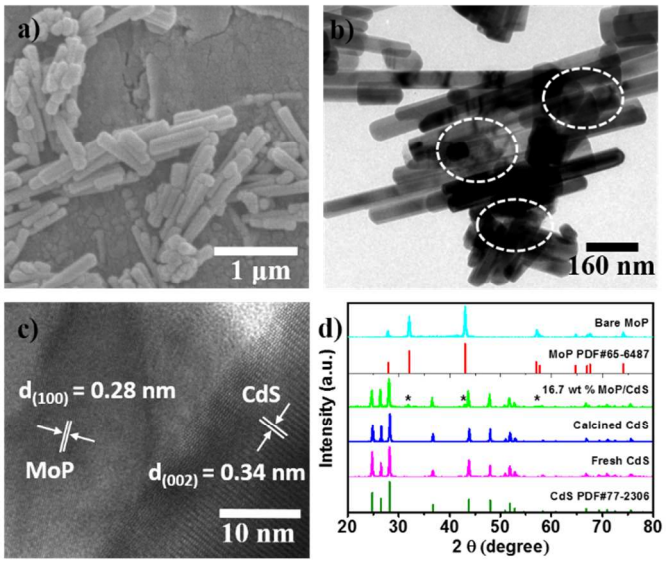

Figure 1. (a) SEM image, (b) TEM image, and (c) HR-TEM image of MoP/CdS NRs (MoP, 16.7 wt %). (d) XRD diffraction patterns of freshly-prepared CdS NRs, calcined CdS NRs, 16.7 wt % MoP/CdS NRs, and MoP. The standard diffraction patterns of CdS and MoP are PDF#77-2306 and PDF#65-6487, respectively. The asterisked positions corresponds to the typical diffraction peaks of MoP.

The intimate attachment of CdS and MoP was further studied by high resolution transmission electron microscopy (HR-TEM) (Figure 1c and Figure S4). As shown in Figure 1c, the HR-TEM image of local CdS NRs/MoP shows that the d-spacings of the lattice fringes are 0.28 nm, corresponding to the (100) plane of MoP.[37, 38] The presence of CdS can be recognized by the (002) lattice distance at 0.34 nm.[32, 42]

The crystalline diffraction patterns of the as-prepared samples were examined by powder X-ray diffraction (Figure 1d). The results show that all the XRD patterns display sharp peaks, indicating good crystallinity of all the samples. The typical crystalline phase diffraction peaks at 2θ = 24.8°, 26.5°, 28.2°, 36.7°, and 47.9° are observed for CdS NRs, corresponding to the (100), (002), (101), (102), and (103) planes of hexagonal CdS (PDF#77-2306), respectively.[32] The diffraction peaks were located at 27.9°, 31.9°, 42.9°, and 73.9° for MoP, probably contributed by the (001), (100), (101), and (201) planes of hexagonal MoP (PDF#65-6487), respectively.[43] Note that when the MoP content is lower than 4 wt % in the hybrid MoP/CdS NRs samples, no obvious diffraction peaks belonging to MoP can be observed. In contrast, the intensities of diffraction peaks at (100), (101), and (110) planes of MoP increase gradually when the MoP content is more than 4 wt % (Figure S5). All the peaks of the CdS NRs show no significant difference, indicating that the presence of MoP does not influence the crystalline phases of CdS NRs. However, the relative intensities of the (311) and (220) planes of the calcined CdS NRs increase when the intensities of (111) and (110) planes decrease (Figure S6). The nitrogen adsorption/desorption isotherm plots of bare CdS NRs, bare MoP, and 16.7 wt % MoP/CdS NRs composite show that their Brunauer–Emmett–Teller (BET) surface areas are 20.49, 40.27, and 21.70 m^2/g, respectively (Figure S7). The DFT pore-size distribution curve of MoP further shows the porous structure has both microporous and mesoporous (Figure S7d). The average microporous pore size is ~1.5 nm, the average mesoporous pore size is ~4 nm, and the larger mesoporous pore size ranges from 20 to 30 nm. The porous structure is probably contributed by citric acid as the chelating agent.[38]

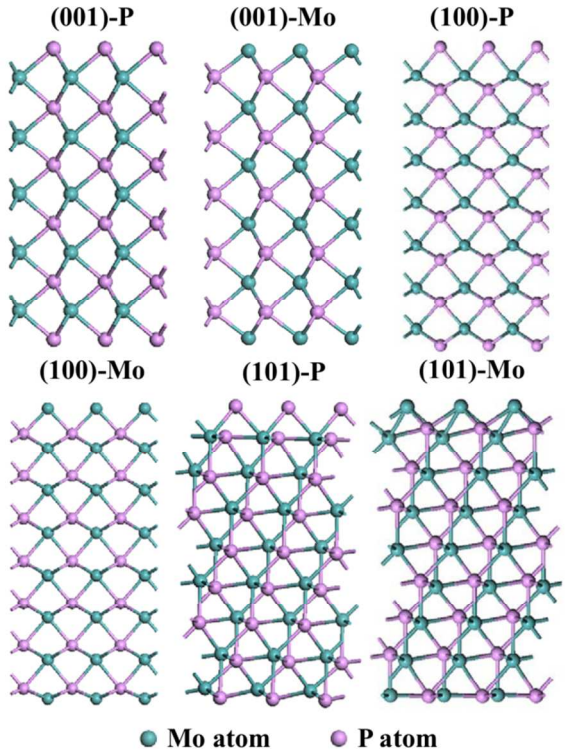

Figure 2. The side view of (001), (100), and (101) surfaces with different atom terminated of MoP.

Table 1. The calculated surface energies and work functions of (001), (100), and (101) surfaces with different atom terminated of MoP.

Surface	(001)-P	(001)-Mo	(100)-P	(100)-Mo	(101)-P	(101)-Mo
Surface energy (eV/Å^2)	0.164	0.492	0.242	0.509	0.221	0.429
Work Function (eV)	5.442	4.090	5.480	4.212	5.199	4.278

To understand the formation of hybrid MoP/CdS NRs, we calculated the surface energies of MoP (001), (100), and (101) surfaces with DFT method (the calculation details can be found in the supporting information). Figure 2 shows the (001), (100), and (101) surfaces with different atom terminated of MoP. As summarized in Table 1, the Mo-terminated surfaces have higher surface energy than that of P-terminated surfaces. Moreover, the (100) surface have the largest surface energy of 0.509 and 0.242 eV/Å^2 for Mo and P-terminated surfaces, respectively. Note that the

surface with high surface energy is unstable and easily disappears. Therefore, the high energy surface of MoP tends to disappear by agglomeration. However, due to the introduction of CdS, the CdS NRs, especially the short CdS NRs, can attach onto the as-prepared MoP surface during the commixture and calcination processes. Thus, the existing high energy surface of MoP can be stabilized by the intimate attachment of MoP and CdS, such as (100) surface.

X-ray photoelectron spectroscopy (XPS) experiments were carried out to elucidate the valence states of individual element and chemical compositions in the as-synthesized samples. The XPS survey spectrum of MoP/CdS NRs shows the existence of Cd, S, Mo, and P elements (Figure S8), which is also confirmed by the energy-dispersive X-ray analysis (EDX) (Figure S9). The C element is the reference and the O element is probably from molybdenum oxides and the absorbed gaseous molecules on the surface. The presence of the S 2p peaks at 161.7 eV/162.76 eV (S $2p_{3/2}/2p_{1/2}$) and the Cd 3d peaks at 411.45 eV/404.76 eV (Cd $3d_{5/2}/3d_{3/2}$) confirms the presence of CdS (Figure S10).[13, 44] As can be seen in the high resolution XPS spectra of MoP (Figure 3a), deconvolution of the Mo 3d spectrum shows two doublets at 229.24 eV and 232.42 eV, corresponding to MoO_2, and peaks appeared at 232.91 eV and 235.46 eV, corresponding to MoO_3.[39] It should be noted that the high oxidation state of Mo could be due to the passivation process during synthesis.[36] This hypothesis is affirmed by the disappearance of the peak of MoO_2 at 229.24 eV and the appearance of a new low-intensity Mo $3d_{5/2}$ peak at 230.36 eV, which probably belongs to MoO_xS_y[45] at the interface of MoP and CdS NRs after the commixture process. The rest of the Mo 3d peaks, located at 228.26 eV and 231.57 eV, are assigned to MoP in agreement with previous reports.[39, 46] In Figure 3b, the high resolution XPS peaks of P 2p shows a doublet at 129.68 eV and 130.54 eV, corresponding to the P character in MoP, while the P $2p_{3/2}$ peak with the binding energy at 134.15 eV represents the typical oxidation peak of phosphorous, such as in PO_4^{3-}, P_2O_5, and H_3PO_3.[47-49] Figures 3c-3d show the high resolution XPS spectrum of Mo 3d in MoP/CdS NRs before photocatalysis. The two peaks centered at 232.53 eV and 235.67 eV can be attributed to the binding energies of Mo $3d_{3/2}$ of MoO_2 and MoO_3, respectively.[39] The binding energy peaks located at 227.83 eV and 231.41 eV are from MoP.[36, 50] The peak located at 226.1 eV is assigned to S 2s in CdS (Figure 3d).[51]

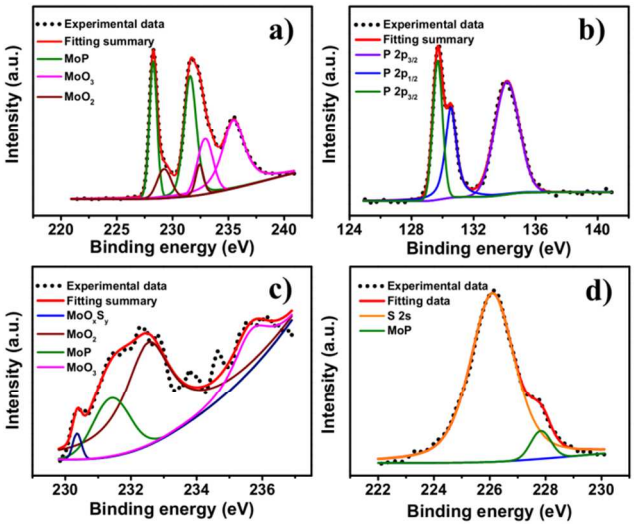

Figure 3. (a) High resolution XPS spectra of Mo 3d; (b) High resolution XPS spectra of P 2p; (c) and (d) are the high resolution XPS spectra of Mo 3d in hybrid MoP/CdS NRs (MoP, 16.7 wt%), and the strong peak located at 226.1 eV is attributed to S 2s.

UV-vis diffuse reflectance absorption spectra analysis was conducted to investigate the optical absorption properties of the as-synthesized samples. Figure 4a shows bare MoP and MoP/CdS NRs samples with different amounts of MoP. It is observed that the adsorption edge of the CdS NRs is at ~530 nm, corresponding to a band gap (Eg) of ~2.36 eV, which is consistent with previous reports.[32, 52] The MoP material shows a flat plot with high adsorption coefficient throughout the UV-vis wavelength range, indicating that MoP exhibits metallic character, which is further evidenced by the valence band (VB) XPS spectrum of MoP (Figure 4b). The valence band edge is located at ~0.15 eV below the Fermi level, confirming the metallic character of MoP. In addition, no significant shift of the absorption edges was observed for the hybrid MoP/CdS NRs materials, while the absorption intensity of the MoP/CdS NRs in the visible region above 530 nm is gradually enhanced with the increasing content of MoP. This observation also indicates that the addition of MoP does not change the CdS lattice, nor as well as the optical absorption properties of CdS NRs.

The calculated band structures and density of state (DOS) confirm the metallic character of MoP. As shown in Figure 4c, MoP is metallic with non-zero DOS crossing the Fermi energy level. The Mo atom, especially the 4d orbital of the Mo atom, contributes the majority state near the Fermi level. Since the 4d orbitals of Mo are partly occupied at the Fermi energy level, it can accept more electrons only with a minor change on the position of the Fermi energy level. Thus, when the photogenerated electrons at the conduction bang (CB) of CdS flow to MoP, the nearly fixed Fermi level of MoP can accept more electrons and maintain its high activity.

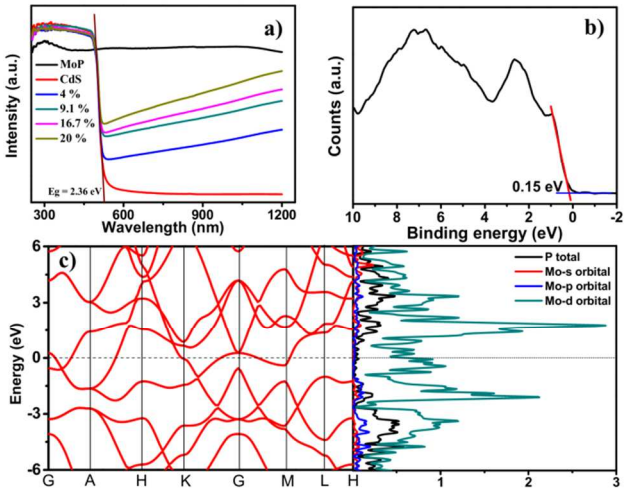

Figure 4. (a) UV-vis diffuse reflectance spectra of MoP/CdS NRs with different amounts of MoP. (b) Valence band of MoP in XPS spectrum. (c) Calculated electronic band structure (left) and density of state (DOS) (right) of MoP.

Based on the calculations, the photocatalytic H_2 production activity of the present hybrid MoP/CdS NRs photocatalyst was evaluated in aqueous solution under visible light (> 420 nm). The system contained 1.0 mg photocatalyst and lactic acid (10 %, v/v) as a sacrificial agent. Figure 5a shows the H_2 production rates of MoP/CdS NRs photocatalysts with different contents of MoP. Pure MoP and CdS NRs were used for comparison. The H_2 production rate of the freshly-prepared CdS NRs without calcination was ~8 $\mu mol \cdot h^{-1} \cdot mg^{-1}$ and the rate of calcined CdS NRs was ~17.8 $\mu mol \cdot h^{-1} \cdot mg^{-1}$. However, no appreciable H_2 was observed when pure MoP was used, indicating that metallic MoP is not an active photocatalyst

in the present system. When mixing only 4 wt % MoP on CdS NRs photocatalyst, an enhanced H_2 production rate was clearly observed (~76 μmol·h^{-1}·mg^{-1}). The rates of H_2 production exhibited a wave-type activity with the increasing amount of MoP. Obviously, an appropriate content of MoP can dramatically improve the photocatalytic activity for H_2 production in the system. A maximal H_2 evolution rate was achieved with the photocatalyst containing 16.7 wt % MoP (~163.2 μmol·h^{-1}·mg^{-1}), which is more than 20 times higher than that of freshly-prepared CdS NRs. The decreasing photocatalytic activity for H_2 production was obtained with a higher MoP content of > 16.7 wt %. Usually, the optimal rate for photocatalytic H_2 production in a metal-semiconductor system can be achieved with a loading content of a cocatalyst less than 10.0 wt %.[13, 42, 53, 54] The high content of the cocatalyst in our present system is probably because some MoP cocatalyst is not uniformly attached to CdS during the mechanical mixing process.

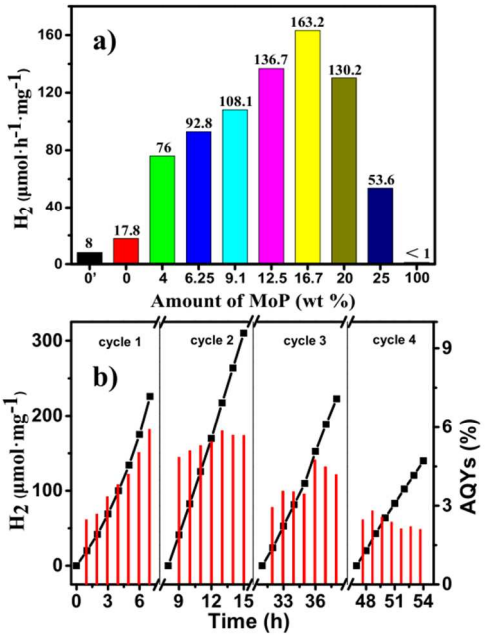

Figure 5. (a) Rate of H_2 evolution from MoP/CdS NRs photocatalysts with different amounts of MoP in a 10 % (v/v) lactic acid aqueous solution at room temperature under visible light (λ > 420 nm). (b) Time courses of H_2 production and apparent quantum yields (AQYs) of 16.7 wt % MoP/CdS NRs photocatalyst under monochromatic 450 nm light irradiation using 1.0 mg photocatalyst in a 20 ml 10 % (v/v) lactic acid aqueous solution at room temperature. Fresh N_2 was bubbled into the vessel in the interval of each cycle to exhaust H_2 gas generated with no additional lactic acid. The reaction suspension was stored in darkness for 1 hours, 16 hours, and 9 hours after cycle 1, cycle 2, and cycle 3, respectively.

The apparent quantum yields (AQYs) for H_2 evolution over 16.7 wt % MoP/CdS NRs photocatalyst were measured under a monochromatic light at 450 nm (±5 nm). N_2 was bubbled into the vessel in the interval of each cycle to exhaust the H_2 gas generated under visible light with no additional sacrificial electron donor. The reaction suspension was stored in darkness for 1 hour, 16 hours, and 9 hours after cycle 1, cycle 2, and cycle 3, respectively. In Figure 5b, the results show that the AQYs in cycle 1 increase gradually with the increasing illumination time. Since the mechanical commixture method inevitably results in an uneven distribution of MoP on CdS NRs, the unattached MoP particles are on a collision course with the CdS NRs during constant stirring, which probably further enhances the activity of photocatalytic H_2 production. The long-term photocatalytic reaction in cycle 2 results in an average AQY of ~5.6 %, demonstrating that MoP/CdS NRs photocatalyst is efficient and stable for H_2 production in aqueous solution. The AQYs of the photocatalyst show a slight decrease in cycle 3 and cycle 4, indicating that long-term soaking in lactic acid solution or the decreasing concentration of lactic acid may lower the photocatalytic activity.

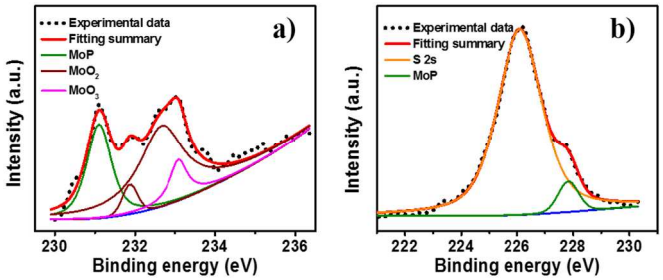

Figure 6. (a) and (b) are the high resolution XPS spectrum of Mo 3d after photocatalysis, and the strong peak located at 226.1 eV is attributed to S 2s.

XPS spectra were further collected to check the stability of the MoP/CdS NRs photocatalyst (Figure 6). The results show that there is no significant change in either MoP or CdS NRs except for the disappearance of the MoO_xS_y character after visible light irradiation for 5 hours, which probably indicates that the electron transfer process occurred in the interface of MoP and CdS NRs (Figure 6a). The binding energies of 231.86 eV/232.67 eV and 233.09 eV are assigned to MoO_2 and MoO_3, respectively. The remaining peaks at 227.83 eV and 231.09 eV are from MoP (Figures 6a-6b).[36, 55] The peak at 226.1 eV after visible light irradiation should be from S 2s in CdS (Figure 6b).[51] All the results suggest that the MoP/CdS NRs photocatalyst has good stability during photocatalysis.

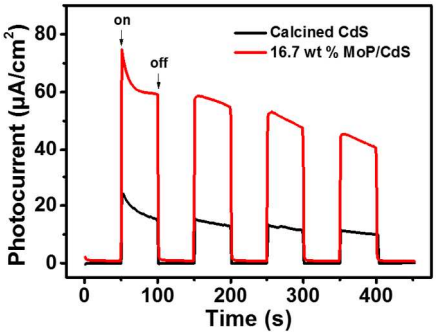

Figure 7. Transient photocurrent responses of calcined CdS NRs and hybrid MoP/CdS NRs photocatalyst under chopped visible light irradiation.

In order to explore the reaction mechanism for photocatalytic H_2 production over MoP/CdS NRs, the transient photocurrent responses of MoP/CdS NRs and CdS NRs were examined (Figure 7). In the dark, no significant photocurrent was observed for both MoP/CdS NRs and calcined CdS NRs. In contrast, both materials show appreciable photocurrents under chopped visible light irradiation (> 420 nm). Impressively, the photocurrent response of MoP/CdS NRs exhibits much higher intensity than that of calcined CdS NRs, revealing that the charge transfer process in MoP/CdS is more efficient. In the photocurrent studies, the electrons might come from hydroxide ions in water. Oxygen production was previously observed on the naked CdS electrode under illumination in a 0.5 M Na_2SO_4 solution.[56] The photogenerated holes in the VB of CdS

might be involved in the oxidation reaction to produce oxygen, accompanied with the photocorrosion of CdS. Due to the inherent photodegradation of CdS, holes produced in the VB migrate to the surface where rapid oxidation of sulfide ions to sulfur,[57-59] leading to a very low efficiency of oxygen production.[56,58] The above result suggests that MoP probably helps the process of charge transfer and subsequently enhances the photocatalytic H_2 production activity.

As shown in Table 1, the Mo-terminated surface work function is located between 4.090 and 4.278 eV, while the P-terminated surface has a higher work function from 5.199 to 5.442 eV. The calculated results indicate that the MoP surface with Mo-terminated has a well-matched Fermi level between the CBM of CdS and the reduction potential (H^+/H_2), but its surface energy is higher. Thus, it is important to carefully control the synthesis of MoP to expose high energy Mo-terminated surface and stabilize the high energy surface. Based on above results and analyses, a tentative mechanism for the enhanced H_2 production activity in the MoP/CdS NRs sample is proposed, as shown in Scheme 1. CdS, an n-type semiconductor (E_g ~2.36 eV), can effectively absorb visible light to excite electrons located at VB to CB, accompanying with the creation of photogenerated electron-hole pairs. MoP displays a metallic character and its Fermi level (about -4.090 to -4.278 eV vs. AVS) is lower than the CBM of CdS (about -3.98 eV vs. AVS) but higher than the proton reduction potential (H^+/H_2, about -4.5 eV vs. AVS).[32] With the introduction of MoP on CdS NRs, a hybrid metal-semiconductor system with typical metal-semiconductor interfaces was thus created. Due to the good Fermi level alignment of MoP and CdS, the photogenerated electrons located at the CB of CdS will facilely transfer to the MoP Fermi level rather than move back to the defect energy levels or lower VB to recombine with holes, resulting in effective separation of electron-hole pairs and reduction of charge recombination. Because of the good carrier mobility of metallic MoP, highly active electrons on the MoP surface will participate in the reduction of protons instead of remaining on the CdS NRs surface, leading to significant enhanced photocatalytic H_2 production and suppressed photocorrosion of CdS. All the results suggest that metallic MoP is an efficient cocatalyst in photocatalysis.

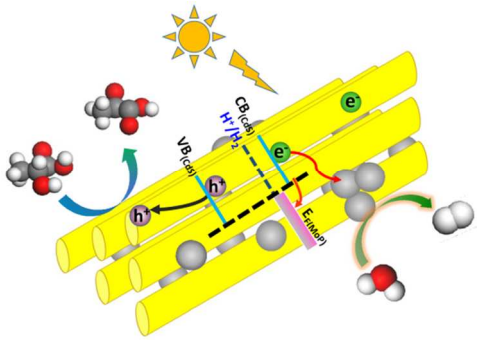

Scheme 1. The reaction mechanism for photocatalytic H_2 evolution using MoP/CdS NRs hybrid.

Conclusions

In conclusion, we have studied the use of MoP as a novel cocatalyst to construct the MoP/CdS NRs photocatalyst, a hybrid metal-semiconductor system, for H_2 production under visible light. The as-synthesized MoP displays metallic character, confirmed by both experimental results and DFT analyses. Under optimal conditions, the MoP/CdS exhibited a H_2 evolution rate of 163.2 $\mu mol \cdot h^{-1} \cdot mg^{-1}$, which is more than 9 times and 20 times higher than that of bare calcined and freshly-prepared CdS NRs, respectively. The maximum apparent quantum yield of ~5.8 % was achieved during excitation at 450 nm. The good Fermi level alignment of MoP and CdS can promote fast charge transfer in the metal-semiconductor interfaces of MoP/CdS, which is responsible for the highly enhanced photocatalytic H_2 production activity.

Acknowledgements

P. D. is financially supported by NSFC (21271166, 21473170), the Fundamental Research Funds for the Central Universities, the Program for New Century Excellent Talents in University (NCET), and the Thousand Young Talents Program. X.W. is supported by National Key Basic Research Program (2012CB922001, 2011CB921404), by NSFC (51172223, 21421063), by Strategic Priority Research Program of CAS (XDB01020300), by Fundamental Research Funds for the Central Universities, and by USTCSCC, SCCAS, Tianjin, and Shanghai Supercomputer Centers.

Notes and references

[a] *Key Laboratory of Materials for Energy Conversion, Chinese Academy of Sciences, Department of Materials Science and Engineering, iChEM (Collaborative Innovation Center of Chemistry for Energy Materials), University of Science and Technology of China, 96 Jinzhai Road, Hefei, Anhui Province, 230026, P. R. China.* [b] *Hefei National Laboratory of Physical Science at the Microscale, University of Science and Technology of China, Hefei, Anhui 230026, China.* [c] *Synergetic Innovation Center of Quantum Information & Quantum Physics, University of Science and Technology of China, Hefei, Anhui 230026, P. R. China.* [d] *School of Chemistry and Chemical Engineering, Anhui University, Hefei 230039, P. R. China.*
Phone/Fax: 86-551-63606207; E-mail: dupingwu@ustc.edu.cn; xjwu@ustc.edu.cn

† Electronic Supplementary Information (ESI) available: Experimental details, SEM image of MoP, SEM image and XPS of CdS, TEM, HR-TEM, XRD, XPS survey data, and EDX data of MoP/CdS. See DOI: 10.1039/c000000x/

1. U. Bach, D. Lupo, P. Comte, J. E. Moser, F. Weissortel, J. Salbeck, H. Spreitzer and M. Gratzel, *Nature*, 1998, **395**, 583-585.
2. S. U. Khan, M. Al-Shahry and W. B. Ingler, Jr., *Science*, 2002, **297**, 2243-2245.
3. T. F. Jaramillo, K. P. Jorgensen, J. Bonde, J. H. Nielsen, S. Horch and I. Chorkendorff, *Science*, 2007, **317**, 100-102.
4. J. Liu, Y. Liu, N. Liu, Y. Han, X. Zhang, H. Huang, Y. Lifshitz, S.-T. Lee, J. Zhong and Z. Kang, *Science*, 2015, **347**, 970-974.
5. Y. Zheng, Y. Jiao, M. Jaroniec and S. Z. Qiao, *Angew. Chem. Int. Ed.*, 2015, **54**, 52-65.
6. J. G. Yu, L. F. Qi and M. Jaroniec, *J. Phys. Chem. C*, 2010, **114**, 13118-13125.
7. S. K. Mohapatra, M. Misra, V. K. Mahajan and K. S. Raja, *J. Phys. Chem. C*, 2007, **111**, 8677-8685.
8. D. I. Enache, J. K. Edwards, P. Landon, B. Solsona-Espriu, A. F. Carley, A. A. Herzing, M. Watanabe, C. J. Kiely, D. W. Knight and G. J. Hutchings, *Science*, 2006, **311**, 362-365.
9. C. Zhu, J. Zeng, J. Tao, M. C. Johnson, I. Schmidt-Krey, L. Blubaugh, Y. Zhu, Z. Gu and Y. Xia, *J. Am. Chem. Soc.*, 2012, **134**, 15822-15831.
10. T. Simon, N. Bouchonville, M. J. Berr, A. Vaneski, A. Adrovic, D. Volbers, R. Wyrwich, M. Doblinger, A. S. Susha, A. L. Rogach, F.

Jackel, J. K. Stolarczyk and J. Feldmann, *Nat. Mater.*, 2014, **13**, 1013-1018.
11. J. Ran, J. Yu and M. Jaroniec, *Green Chem.*, 2011, **13**, 2708-2713.
12. W. Zhang, Y. Wang, Z. Wang, Z. Zhong and R. Xu, *Chem. Commun.*, 2010, **46**, 7631-7633.
13. X. Zong, H. Yan, G. Wu, G. Ma, F. Wen, L. Wang and C. Li, *J. Am. Chem. Soc.*, 2008, **130**, 7176-7177.
14. M. Higashi, K. Domen and R. Abe, *J. Am. Chem. Soc.*, 2012, **134**, 6968-6971.
15. P. Sabatier, *Ber. Dtsch. Chem. Ges.*, 1911, **44**, 1984-2001.
16. P. Liu and J. A. Rodriguez, *Catal. Lett.*, 2003, **91**, 247-252.
17. P. A. Aegerter, W. W. C. Quigley, G. J. Simpson, D. D. Ziegler, J. W. Logan, K. R. McCrea, S. Glazier and M. E. Bussell, *J. Catal.*, 1996, **164**, 109-121.
18. D. Kanama, S. T. Oyama, S. Otani and D. F. Cox, *Surf. Sci.*, 2004, **552**, 8-16.
19. S. J. Sawhill, D. C. Phillips and M. E. Bussell, *J. Catal.*, 2003, **215**, 208-219.
20. P. Liu, J. A. Rodriguez, T. Asakura, J. Gomes and K. Nakamura, *J. Phys. Chem. B*, 2005, **109**, 4575-4583.
21. E. J. Popczun, J. R. McKone, C. G. Read, A. J. Biacchi, A. M. Wiltrout, N. S. Lewis and R. E. Schaak, *J. Am. Chem. Soc.*, 2013, **135**, 9267-9270.
22. A. Han, S. Jin, H. Chen, H. Ji, Z. Sun and P. Du, *J. Mater. Chem. A*, 2015, **3**, 1941-1946.
23. Y. Pan, Y. Liu, J. Zhao, K. Yang, J. Liang, D. Liu, W. Hu, D. Liu, Y. Liu and C. Liu, *J. Mater. Chem. A*, 2015, **3**, 1656-1665.
24. Z. Huang, Z. Chen, Z. Chen, C. Lv, H. Meng and C. Zhang, *ACS nano*, 2014, **8**, 8121-8129.
25. E. J. Popczun, C. G. Read, C. W. Roske, N. S. Lewis and R. E. Schaak, *Angew. Chem. Int. Ed.*, 2014, **53**, 5427-5430.
26. Q. Liu, J. Tian, W. Cui, P. Jiang, N. Cheng, A. M. Asiri and X. Sun, *Angew. Chem. Int. Ed.*, 2014, **53**, 6710-6714.
27. Z. Pu, Q. Liu, P. Jiang, A. M. Asiri, A. Y. Obaid and X. Sun, *Chem. Mater.*, 2014, **26**, 4326-4329.
28. J. Tian, N. Cheng, Q. Liu, W. Xing and X. Sun, *Angew. Chem. Int. Ed.*, 2015, **54**, 5493-5497.
29. J. Tian, Q. Liu, A. M. Asiri and X. Sun, *J. Am. Chem. Soc.*, 2014, **136**, 7587-7590.
30. P. Jiang, Q. Liu, Y. Liang, J. Tian, A. M. Asiri and X. Sun, *Angew. Chem. Int. Ed.*, 2014, **53**, 12855-12859.
31. Z. Zhang, B. Lu, J. Hao, W. Yang and J. Tang, *Chem. Commun.*, 2014, **50**, 11554-11557.
32. Z. Sun, Q. Yue, J. Li, J. Xu, H. Zheng and P. Du, *J. Mater. Chem. A*, 2015, **3**, 10243-10247.
33. D. C. Phillips, S. J. Sawhill, R. Self and M. E. Bussell, *J. Catal.*, 2002, **207**, 266-273.
34. T. Zhao, Z. Zhao, F. Li, G. Sun and C. Li, *Petrochem. Technol.*, 2004, **10**, 004.
35. D. Song, W. Guo, Y. Li, H. Ren and Q. Zhou, *Chem. Ind. Eng. Prog.*, 2009, **5**, 024.
36. T. Wang, K. Du, W. Liu, Z. Zhu, Y. Shao and M. Li, *J. Mater. Chem. A*, 2015, **3**, 4368-4373.
37. W. Cui, Q. Liu, Z. Xing, A. M. Asiri, K. A. Alamry and X. Sun, *Appl. Catal., B*, 2015, **164**, 144-150.
38. Z. Xing, Q. Liu, A. M. Asiri and X. Sun, *Adv. Mater.*, 2014, **26**, 5702-5707.
39. P. Xiao, M. A. Sk, L. Thia, X. M. Ge, R. J. Lim, J. Y. Wang, K. H. Lim and X. Wang, *Energy Environ. Sci.*, 2014, **7**, 2624-2629.
40. X. Chen, D. Wang, Z. Wang, P. Zhou, Z. Wu and F. Jiang, *Chem. Commun.*, 2014, **50**, 11683-11685.
41. C. Stinner, R. Prins and T. Weber, *J. Catal.*, 2000, **191**, 438-444.
42. Z. Yan, X. Yu, A. Han, P. Xu and P. W. Du, *J. Phys. Chem. C*, 2014, **118**, 22896-22903.
43. Z. Yao, M. Li, X. Wang, X. Qiao, J. Zhu, Y. Zhao, G. Wang, J. Yin and H. Wang, *Dalton Trans.*, 2015, **44**, 5503-5509.
44. X. G. Peng, M. C. Schlamp, A. V. Kadavanich and A. P. Alivisatos, *J. Am. Chem. Soc.*, 1997, **119**, 7019-7029.
45. L. Benoist, D. Gonbeau, G. Pfisterguillouzo, E. Schmidt, G. Meunier and A. Levasseur, *Thin Solid Films*, 1995, **258**, 110-114.
46. J. Bai, X. Li, A. J. Wang, R. Prins and Y. Wang, *J. Catal.*, 2012, **287**, 161-169.
47. E. Fluck and D. Weber, *Z. Naturforsch., B*, 1974, **29**, 603-607.
48. A. Montesinos-Castellanos, T. A. Zepeda, B. Pawelec, J. L. G. Fierro and J. A. de los Reyes, *Chem. Mater.*, 2007, **19**, 5627-5636.
49. M. Latorre-Sánchez, A. Primo and H. García, *Angew. Chem. Int. Ed.*, 2013, **52**, 11813-11816.
50. I. I. Abu and K. J. Smith, *Catal. Today*, 2007, **125**, 248-255.
51. V. Bhide, S. Salkalachen, A. Rastog, C. Rao and M. Hegde, *J. Phys. D: Appl. Phys.*, 1981, **14**, 1647.
52. J. S. Jang, U. A. Joshi and J. S. Lee, *J. Phys. Chem. C*, 2007, **111**, 13280-13287.
53. H. Yan, J. Yang, G. Ma, G. Wu, X. Zong, Z. Lei, J. Shi and C. Li, *J. Catal.*, 2009, **266**, 165-168.
54. J. S. Jang, D. J. Ham, N. Lakshminarasimhan, W. Y. Choi and J. S. Lee, *Appl. Catal., A*, 2008, **346**, 149-154.
55. V. M. L. Whiffen and K. J. Smith, *Energy Fuels*, 2010, **24**, 4728-4737.
56. A. J. Frank and K. Honda, *J. Phys. Chem.*, 1982, **86**, 1933-1935.
57. H. Gerischer, *J. Electroanal. Chem.* , 1975, **58**, 263-274.
58. D. Meissner, I. Lauermann, R. Memming and B. Kastening, *J. Phys. Chem.*, 1988, **92**, 3484-3488.
59. D. Meissner, R. Memming and B. Kastening, *J. Phys. Chem.*, 1988, **92**, 3476-3483.

.

TOC Figure

The present study showed that MoP is a stable and highly active cocatalyst to promote photocatalytic H_2 production in water when attaching on the semiconductor surface